A Neural Network Approach for an Automatic Detection and Localization of an Open Phase Circuit of a Five-Phase Induction Machine Used in a Drivetrain of an Electric Vehicle

Saad Chahba, Rabia Sehab, Ahmad Akrad, Cristina Morel

A Neural Network Approach for an Automatic Detection and Localization of an Open Phase Circuit of a Five-Phase Induction Machine Used in a Drivetrain of an Electric Vehicle

Conference Paper · July 2022

DOI: 10.1109/ICCAD55197.2022.9853930

4 authors:

Saad Chahba
Ecole Supérieure des Techniques Aéronautiques et de Construction Automobile

Rabia Sehab
Ecole Supérieure des Techniques Aéronautiques et de Construction Automobile

Ahmad Akrad
Ecole Supérieure des Techniques Aéronautiques et de Construction Automobile

Cristina Morel
Ecole Supérieure des Techniques Aéronautiques et de Construction Automobile

2022 International Conference on Control, Automation and Diagnosis (ICCAD) | 978-1-6654-9794-7/22/$31.00 ©2022 IEEE | DOI: 10.1109/ICCAD55197.2022.9853930

A Neural Network Approach for an Automatic Detection and Localization of an Open Phase Circuit of a Five-Phase Induction Machine Used in a Drivetrain of an Electric Vehicle

Saad CHAHBA
ESTACA Engineering School
Laval, France
saad.chahba@estaca.fr

Rabia SEHAB
ESTACA Engineering School
Laval, France
rabia.sehab@estaca.fr

Ahmad AKRAD
ESTACA Engineering School
Laval, France
ahmad.akrad@estaca.fr

Cristina MOREL
ESTACA Engineering School
Laval, France
cristina.morel@estaca.fr

***Abstract*— Nowadays, the electric machines used in urban electric vehicles are, in most cases, three-phase electric machines with or without a magnet in the rotor. Permanent Magnet Synchronous Machine (PMSM) and Induction Machine (IM) are the main components of drive trains of electric and hybrid vehicles. These machines have very good performance in healthy operation mode, but they are not redundant to ensure safety in faulty operation mode. Faced with the continued growth in the demand for electric vehicles in the automotive market, improving the reliability of electric vehicles is necessary over the lifecycle of the electric vehicle. Multiphase electric machines respond well to this constraint because, on the one hand, they have better robustness in the event of a breakdown (opening of a phase, opening of an arm of the power stage, intern-turn short circuit) and, on the other hand, better power density. In this work, a diagnosis approach using a neural network for an open circuit fault or more of a five-phase induction machine is developed. Validation on the simulator of the vehicle drivetrain, at reduced power, is carried out, creating one and more open circuit stator phases showing the efficiency and the reliability of the new approach to detect and to locate on-line one or more open phases of a five-induction machine.**

Keywords— Electric vehicle drivetrain, Multiphase Drives, Induction Machine, Control, Open Circuit (OC) Fault Diagnosis, Artificial Neural Network.

I. INTRODUCTION

Rotating electrical machines with a number of phases higher than three (n > 3) are commonly referred to in the literature as multiphase machines. These electrical machines fed by voltage source inverters (VSI), in comparison with classical three phases machines, gain more degrees of freedom for design and control in healthy mode and in degraded mode where operational safety is always guaranteed. Interest in multiphases machines for variable speed electric traction application has only increased significantly in recent decades. This is thanks to developments in certain specific fields such as power electronics converters and digital signal processors. Another reason for this emergence is that the development of in-depth theories on multiphase machines have been considerably advanced [1]. Fig. 1 gives the structure of an electric drivetrain in which a multiphase machine with a number of phases n is supplied by an inverter with n-arms.

Based on the spatial displacement between two adjacent phases, multiphases machines can be classified as symmetrical (with a spatial phase shift angle of $2\pi/n$) and asymmetric (with several groupings of phases such as two groupings of three phases for one machine six-phase) [2], [3].

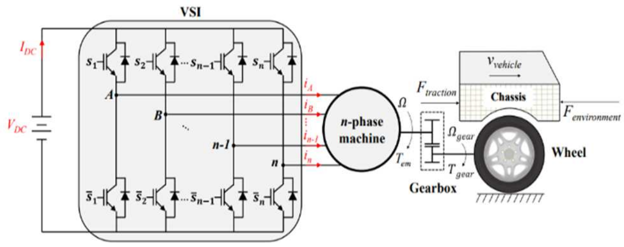

Fig. 1 Architecture of a vehicle drivetrain using a multiphase machine supplied by an inverter with n arms

If rotor construction is considered, there are three true types of technologies: an induction machine, a permanent magnet synchronous machine, and switched reluctance machine. The asynchronous machine, often called induction machine, having a squirrel cage rotor is attractive due to low-cost materials. However, the permanent magnet synchronous machine allows, thanks to the magnetic field created by the permanent magnets, to generate a high power and torque density with a very high efficiency compared to other technologies [4]. The switched reluctance machine has a non-ferromagnetic rotor and robust with significant salience. Like synchronous machines with permanent magnets, it has a stator made of ferromagnetic material comprising teeth on which coils are wound which create the magnetic field. The absence of permanent magnets allows the rotor to be temperature independent and shock and vibration resistant. By its rotor structure and the independence between its phases, this machine is tolerant to intrinsic faults [5].

In this paper, we will be interested in the multiphase induction machine for electric vehicle applications, as the induction machine remains the most suitable candidate. Indeed, the induction machine in comparison with other technologies, allows the obtaining of improved power distribution per phase, decreasing the rated current through each phase as the number of phases increases for a given rated power, allowing less damage to converters, improved torque density and fault tolerance capability. Indeed, an induction machine with n-phases with one or more faulty phases can operate without requiring external equipment as long as the number of faulty phases is not greater than (n - 3) [6]. In this paper, a five-phase induction machine is chosen in the drive train of an electric vehicle, but in general case the choice of any phase number depends essentially on the fault number that can be tolerated in the system, power rate and degrees of freedom for the design and control.

In comparison with conventional three-phase machines, multiphase machines allow four main advantages to be satisfied [7]-[10]:

- Low nominal power per phase for safe electric vehicles: For electric vehicle applications, user safety is important. In this case, a low voltage standard (<48 V) can be a solution to guarantee electrical safety. Low voltage multiphase machines can avoid high voltage electric shock as well as complex and costly requirements for circuit isolation and power electronic devices. Therefore, the protection costs are reduced.
- Fault Tolerant: Fault tolerance is one of the main advantages of multiphase machines, because their redundant design allows them to have more degrees of freedom (DoF) for control than conventional three-phase machines. This functionality allows the maintenance of persistent operation of multiphases machines.
- Low torque ripples: With a multiphase machine, it is possible to obtain a constant torque by imposing constant d-q currents in different reference planes. However, a three-phase machine requires the classical constraint on sinusoidal electromagnetic back electromotive force and currents (in the case of PMSM). Therefore, a multiphase machine leads to less design constraints than a three-phase machine.
- More configuration possibilities for the stator winding: When an inverter is defined with a given maximum current and bus voltage, changes in the connection of the machine windings allow the torque-speed characteristic to be varied with a flux-weakening approach.

Fig. 2 shows the possibilities of stator winding configurations for a 5-phase machine and their effect on the Torque-Speed characteristic.

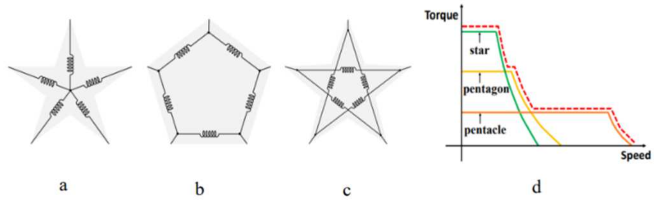

Fig. 2 Stator winding configurations for a machine with five phases: star (a), pentagon (b), pentacle (c) and corresponding torque-speed characteristics (d)

In the literature, research work concerning fault detection and isolation (FDI) based on artificial intelligence techniques, applied to multiphases machines, currently remain very limited, as most of those works are oriented for classic three-phase systems. For instance, reviews of FDI methods can be classified as model-based methods [11], signal based methods [12], [13] or data driven based methods [14], [15]. The first ones need an accurate system model to achieve a robust algorithm. The second ones require the measurement of inverter outputs (currents or voltages). Methods based on voltage analysis have a major drawback because extra hardware or sensors are usually needed for real time implementation. Current-based methods have been used for fault detection and localization for conventional three-phase systems. However, these methods remain incomplete, in particular as regards the transition to multiphase systems [12].

Data driven based methods remain more interesting than the other techniques and especially with the development of Internet of Things, wireless communications, e-commerce, and smart manufacturing, the amount of data collection has grown in an exponential manner. Beyond technological developments, these tools allow greater flexibility in relation to fault processing, as well as obtaining faster detection time. It is the reason why in this paper, we focused on artificial neural network techniques for diagnosis of open phase fault in the inverter side.

The algorithm proposed in this paper is based on the analysis of currents on the stationary plane (α-β), by integrating the Fourier transform to extract the characteristics that define each operating mode, based on this processing we have built database on which the neural networks was trained for the detection and location of OC faults on any phase of the inverter.

In the first section, a five-phase induction machine model is presented with a velocity control using indirect rotor field-oriented control with star topology of the stator winding. However, a simulator of the vehicle drive is developed, and a validation is carried out in healthy operation mode using a velocity mission profile. The second section is devoted to the simulation of an open circuit fault and its effect on the dynamic behavior of the vehicle drivetrain (electric and mechanical variables). In the third section, a diagnosis is carried out and an algorithm is developed using Multi-Layer Perceptron (MLP) neural network for fault detection and location of an open circuit phase or more. Finally, in the last section, a validation is performed online by simulation to show the efficiency and the reliability of the proposed algorithm for detecting and locating an open circuit in any arm of the inverter.

II. Indirect Rotor Field Oriented Control of the Five-Phase Induction Machine

A. *Structure of the Five-phase IM and the VSI*

The considered multiphase system is composed by a five-phase induction machine; with star topology in the stator winding, a voltage source inverter (VSI); the control system which includes the protection and diagnostic functionalities; and an isolated DC-source. The VSI consists of the parallel connection of five-leg inverter, each leg is composed of two transistors (T_k, T_{k+5}, $k = 1,2,3,4,5$). In the next parts, the five-phase system model will be presented, as well as the control technique based on the indirect field oriented control method.

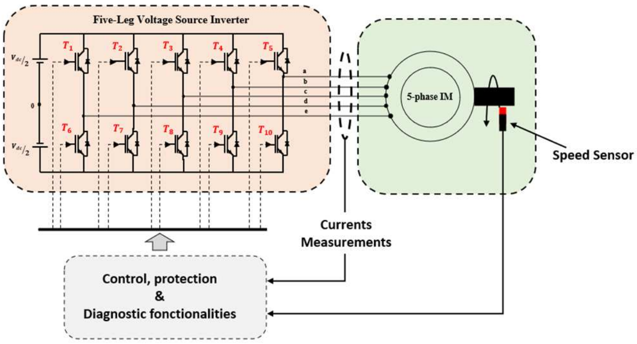

Fig. 3 Structure of the 5-phase electric drive

B. *Model of the five-phase induction machine*

The mathematical model of the 5-phase symmetric induction machine can be modeled by the following set of differential equations, obtained by analyzing the magnetic coupling of the stator and rotor circuits, observed from the stator side [16]:

$$[v_s] = [R_s]\cdot[i_s] + \frac{d}{dt}[\lambda_s] = [R_s]\cdot[i_s] + [L_{ss}]\frac{d}{dt}[i_s] + \frac{d}{dt}([L_{sr}(\theta)]\cdot[i_r]) \quad (1)$$

$$[v_r] = [R_r]\cdot[i_r] + \frac{d}{dt}[\lambda_r] = [R_r]\cdot[i_r] + [\mathrm{L_{rr}}]\frac{d}{dt}[i_r] + \frac{d}{dt}([L_{rs}(\theta)]\cdot[i_s]) \quad (2)$$

$$\theta = \int_0^t \omega_r dt \quad (3)$$

In these equations v, i and λ denote the voltage, current and flux variables respectively, while the subscripts s and r respectively identify the stator and rotor variables. The instantaneous position of the rotor with respect to the stator is represented by θ, while ω_r is the electrical pulsation of the rotor. The voltage, current and flux vectors are defined in (4-9), being the variables corresponding to each phase represented by the indices a, b, c, d and e where we can note that the phase voltages of the rotor are zero because we consider the case of an induction squirrel cage machine.

$$[v_s] = [v_{sa} \quad v_{sb} \quad v_{sc} \quad v_{sd} \quad v_{se}]^T \quad (4)$$

$$[v_r] = [0 \quad 0 \quad 0 \quad 0 \quad 0]^T \quad (5)$$

$$[i_s] = [i_{sa} \quad i_{sb} \quad i_{sc} \quad i_{sd} \quad i_{se}]^T \quad (6)$$

$$[i_r] = [i_{ra} \quad i_{rb} \quad i_{rc} \quad i_{rd} \quad i_{re}]^T \quad (7)$$

$$[\lambda_s] = [\lambda_{sa} \quad \lambda_{sb} \quad \lambda_{sc} \quad \lambda_{sd} \quad \lambda_{se}]^T \quad (8)$$

$$[\lambda_r] = [\lambda_{ra} \quad \lambda_{rb} \quad \lambda_{rc} \quad \lambda_{rd} \quad \lambda_{re}]^T \quad (9)$$

- Clarke decoupled model

The transformation matrix applied to the model based on the phase variables is presented in Equation (10), obtaining the new variables in the stationary frame in Equations (11-14) [16]:

$$C_5 = \frac{2}{5}\begin{bmatrix} 1 & \cos(\vartheta) & \cos(2\vartheta) & \cos(3\vartheta) & \cos(4\vartheta) \\ 0 & \sin(\vartheta) & \sin(2\vartheta) & \sin(3\vartheta) & \sin(4\vartheta) \\ 1 & \cos(2\vartheta) & \cos(4\vartheta) & \cos(6\vartheta) & \cos(8\vartheta) \\ 0 & \sin(2\vartheta) & \sin(4\vartheta) & \sin(6\vartheta) & \sin(8\vartheta) \\ \frac{1}{2} & \frac{1}{2} & \frac{1}{2} & \frac{1}{2} & \frac{1}{2} \end{bmatrix} \quad (10)$$

$$\begin{bmatrix} v_{s\alpha} \\ v_{s\beta} \\ v_{sx} \\ v_{sy} \\ v_{sz} \end{bmatrix} = R_s \cdot \begin{bmatrix} i_{s\alpha} \\ i_{s\beta} \\ i_{sx} \\ i_{sy} \\ i_{sz} \end{bmatrix} + \frac{d}{dt}\begin{bmatrix} \lambda_{s\alpha} \\ \lambda_{s\beta} \\ \lambda_{sx} \\ \lambda_{sy} \\ \lambda_{sz} \end{bmatrix} \quad (11)$$

$$\begin{bmatrix} 0 \\ 0 \\ 0 \\ 0 \\ 0 \end{bmatrix} = R_r \cdot \begin{bmatrix} i_{r\alpha} \\ i_{r\beta} \\ i_{rx} \\ i_{ry} \\ i_{rz} \end{bmatrix} + \frac{d}{dt}\begin{bmatrix} \lambda_{r\alpha} \\ \lambda_{r\beta} \\ \lambda_{rx} \\ \lambda_{ry} \\ \lambda_{rz} \end{bmatrix} + \begin{bmatrix} 0 & \omega_r & 0 & 0 & 0 \\ -\omega_r & 0 & 0 & 0 & 0 \\ 0 & 0 & 0 & 0 & 0 \\ 0 & 0 & 0 & 0 & 0 \\ 0 & 0 & 0 & 0 & 0 \end{bmatrix} \cdot \begin{bmatrix} \lambda_{r\alpha} \\ \lambda_{r\beta} \\ \lambda_{rx} \\ \lambda_{ry} \\ \lambda_{rz} \end{bmatrix} \quad (12)$$

$$\begin{bmatrix} \lambda_{s\alpha} \\ \lambda_{s\beta} \\ \lambda_{sx} \\ \lambda_{sy} \\ \lambda_{sz} \end{bmatrix} = \begin{bmatrix} L_s & 0 & 0 & 0 & 0 \\ 0 & L_s & 0 & 0 & 0 \\ 0 & 0 & L_{ls} & 0 & 0 \\ 0 & 0 & 0 & L_{ls} & 0 \\ 0 & 0 & 0 & 0 & L_{ls} \end{bmatrix} \cdot \begin{bmatrix} i_{s\alpha} \\ i_{s\beta} \\ i_{sx} \\ i_{sy} \\ i_{sz} \end{bmatrix} + \begin{bmatrix} L_m & 0 & 0 & 0 & 0 \\ 0 & L_m & 0 & 0 & 0 \\ 0 & 0 & 0 & 0 & 0 \\ 0 & 0 & 0 & 0 & 0 \\ 0 & 0 & 0 & 0 & 0 \end{bmatrix} \cdot \begin{bmatrix} i_{r\alpha} \\ i_{r\beta} \\ i_{rx} \\ i_{ry} \\ i_{rz} \end{bmatrix} \quad (13)$$

$$\begin{bmatrix} \lambda_{r\alpha} \\ \lambda_{r\beta} \\ \lambda_{rx} \\ \lambda_{ry} \\ \lambda_{rz} \end{bmatrix} = \begin{bmatrix} L_r & 0 & 0 & 0 & 0 \\ 0 & L_r & 0 & 0 & 0 \\ 0 & 0 & L_{lr} & 0 & 0 \\ 0 & 0 & 0 & L_{lr} & 0 \\ 0 & 0 & 0 & 0 & L_{lr} \end{bmatrix} \cdot \begin{bmatrix} i_{r\alpha} \\ i_{r\beta} \\ i_{rx} \\ i_{ry} \\ i_{rz} \end{bmatrix} + \begin{bmatrix} L_m & 0 & 0 & 0 & 0 \\ 0 & L_m & 0 & 0 & 0 \\ 0 & 0 & 0 & 0 & 0 \\ 0 & 0 & 0 & 0 & 0 \\ 0 & 0 & 0 & 0 & 0 \end{bmatrix} \cdot \begin{bmatrix} i_{s\alpha} \\ i_{s\beta} \\ i_{sx} \\ i_{sy} \\ i_{sz} \end{bmatrix} \quad (14)$$

In this frame, the electromagnetic torque expression is given by:

$$T_{em} = p \cdot \frac{5}{2} \cdot L_m \cdot (i_{r\alpha} \cdot i_{s\beta} - i_{r\beta} \cdot i_{s\alpha}) \quad (15)$$

The variables in the $x - y$ subspace, as well as in the z component, are not present in the torque equation, showing that the useful transformation of energy only occurs in the subspace $\alpha\text{–}\beta$.

- Model in the $d\text{–}q$ reference frame

By applying the Park transformation to obtain the model in the rotating frame of reference $d - q$ defined in Equations (16-17), the stator and rotor variables in the new rotating reference frame are given by Equations (18-21) [16]:

$$[P_{s5}] = \begin{bmatrix} \cos(\theta_a) & \sin(\theta_a) & 0 & 0 & 0 \\ -\sin(\theta_a) & \cos(\theta_a) & 0 & 0 & 0 \\ 0 & 0 & 1 & 0 & 0 \\ 0 & 0 & 0 & 1 & 0 \\ 0 & 0 & 0 & 0 & 1 \end{bmatrix} \quad (16)$$

$$[P_{r5}] = \begin{bmatrix} \cos(\delta) & \sin(\delta) & 0 & 0 & 0 \\ -\sin(\delta) & \cos(\delta) & 0 & 0 & 0 \\ 0 & 0 & 1 & 0 & 0 \\ 0 & 0 & 0 & 1 & 0 \\ 0 & 0 & 0 & 0 & 1 \end{bmatrix} \quad (17)$$

$$\begin{bmatrix} v_{sd} \\ v_{sq} \\ v_{sx} \\ v_{sy} \\ v_{sz} \end{bmatrix} = R_s \cdot \begin{bmatrix} i_{sd} \\ i_{sq} \\ i_{sx} \\ i_{sy} \\ i_{sz} \end{bmatrix} + \frac{d}{dt}\begin{bmatrix} \lambda_{sd} \\ \lambda_{sq} \\ \lambda_{sx} \\ \lambda_{sy} \\ \lambda_{sz} \end{bmatrix} + \begin{bmatrix} 0 & -\omega_a & 0 & 0 & 0 \\ \omega_a & 0 & 0 & 0 & 0 \\ 0 & 0 & 0 & 0 & 0 \\ 0 & 0 & 0 & 0 & 0 \\ 0 & 0 & 0 & 0 & 0 \end{bmatrix} \cdot \begin{bmatrix} \lambda_{rd} \\ \lambda_{rq} \\ \lambda_{rx} \\ \lambda_{ry} \\ \lambda_{rz} \end{bmatrix} \quad (18)$$

$$\begin{bmatrix} 0 \\ 0 \\ 0 \\ 0 \\ 0 \end{bmatrix} = R_r \cdot \begin{bmatrix} i_{r\alpha} \\ i_{r\beta} \\ i_{rx} \\ i_{ry} \\ i_{rz} \end{bmatrix} + \frac{d}{dt}\begin{bmatrix} \lambda_{rd} \\ \lambda_{rq} \\ \lambda_{rx} \\ \lambda_{y} \\ \lambda_{rz} \end{bmatrix} + \begin{bmatrix} 0 & \omega_{sl} & 0 & 0 & 0 \\ -\omega_{sl} & 0 & 0 & 0 & 0 \\ 0 & 0 & 0 & 0 & 0 \\ 0 & 0 & 0 & 0 & 0 \\ 0 & 0 & 0 & 0 & 0 \end{bmatrix} \cdot \begin{bmatrix} \lambda_{rd} \\ \lambda_{rq} \\ \lambda_{rx} \\ \lambda_{ry} \\ \lambda_{rz} \end{bmatrix} \quad (19)$$

$$\begin{bmatrix} \lambda_{sd} \\ \lambda_{sq} \\ \lambda_{sx} \\ \lambda_{sy} \\ \lambda_{sz} \end{bmatrix} = \begin{bmatrix} L_s & 0 & 0 & 0 & 0 \\ 0 & L_s & 0 & 0 & 0 \\ 0 & 0 & L_{ls} & 0 & 0 \\ 0 & 0 & 0 & L_{ls} & 0 \\ 0 & 0 & 0 & 0 & L_{ls} \end{bmatrix} \cdot \begin{bmatrix} i_{sd} \\ i_{sq} \\ i_{sx} \\ i_{sy} \\ i_{sz} \end{bmatrix} + \begin{bmatrix} L_m & 0 & 0 & 0 & 0 \\ 0 & L_m & 0 & 0 & 0 \\ 0 & 0 & 0 & 0 & 0 \\ 0 & 0 & 0 & 0 & 0 \\ 0 & 0 & 0 & 0 & 0 \end{bmatrix} \cdot \begin{bmatrix} i_{rd} \\ i_{rq} \\ i_{rx} \\ i_{ry} \\ i_{rz} \end{bmatrix} \quad (20)$$

$$\begin{bmatrix}\lambda_{rd}\\ \lambda_{rq}\\ \lambda_{rx}\\ \lambda_{ry}\\ \lambda_{rz}\end{bmatrix}=\begin{bmatrix}L_r & 0 & 0 & 0 & 0\\ 0 & L_r & 0 & 0 & 0\\ 0 & 0 & L_{lr} & 0 & 0\\ 0 & 0 & 0 & L_{lr} & 0\\ 0 & 0 & 0 & 0 & L_{lr}\end{bmatrix}\cdot\begin{bmatrix}i_{rd}\\ i_{rq}\\ i_{rx}\\ i_{ry}\\ i_{rz}\end{bmatrix}+\begin{bmatrix}L_m & 0 & 0 & 0 & 0\\ 0 & L_m & 0 & 0 & 0\\ 0 & 0 & 0 & 0 & 0\\ 0 & 0 & 0 & 0 & 0\\ 0 & 0 & 0 & 0 & 0\end{bmatrix}\cdot\begin{bmatrix}i_{sd}\\ i_{sq}\\ i_{sx}\\ i_{sy}\\ i_{sz}\end{bmatrix} \tag{21}$$

Thus, the electromagnetic torque generated is defined by the following expression:

$$T_{em}=p\cdot\frac{n}{2}\cdot L_m\cdot(i_{rd}\cdot i_{sq}-i_{rq}\cdot i_{sd}) \tag{22}$$

C. *Indirect Rotor Field Oriented Control*

The control by orientation of the rotor field consists in achieving a decoupling between the magnitudes generating the electromagnetic torque and the rotor field. In this case, the rotor field component is aligned with the d axis, so the rotor flux in the q axis is zero [17], [18]:

$$\lambda_{rd}=L_r\cdot i_{rd}+L_m\cdot i_{sd}\;\longrightarrow\; i_{rd}=\frac{1}{L_r}(\lambda_{rd}-L_m\cdot i_{sd}) \tag{23}$$

$$\lambda_{rq}=0=L_r\cdot i_{rq}+L_m\cdot i_{sq}\;\longrightarrow\; i_{rd}=-\frac{L_m}{L_r}\cdot i_{sd} \tag{24}$$

$$\frac{d\lambda_{rq}}{dt}=0 \tag{25}$$

By substituting (23)-(25) in rotor voltage Equation (19) and in torque Equation (22), we obtain:

$$\tau_r\cdot\frac{d\lambda_{rd}}{dt}+\lambda_{rd}=L_m\cdot i_{sd} \tag{26}$$

$$\omega_{sl}\cdot\tau_r\cdot\lambda_{rd}=L_m\cdot i_{sq} \tag{27}$$

$$T_{em}=p\cdot\frac{5}{2}\cdot\frac{L_m}{L_r}\cdot\lambda_{rd}\cdot i_{sq} \tag{28}$$

$$\tau_r=\frac{L_r}{R_r} \tag{29}$$

Where τ_r represents the rotor time constant. The electromagnetic torque represented by (28) shows that it can be controlled by changing the stator reference current i_{sq} and keeping the rotor field λ_{rd} constant below synchronism. By analyzing (26), we can affirm that the rotor field is independent of the current i_{sq}, responsible for the torque production, and that the value of the rotor flux is determined only by the stator current i_{sd}.

The block diagram of the indirect rotor field-oriented control (IRFOC) for a five-phase induction machine with distributed windings is shown in Fig. 4. The technique is based on three independent control loops for speed, rotor field and torque. The use of proportional-integral (PI) controllers gives the controller robustness against the main drawback of this method of control, which is the need to know the parameters of the machine in order to obtain orientation.

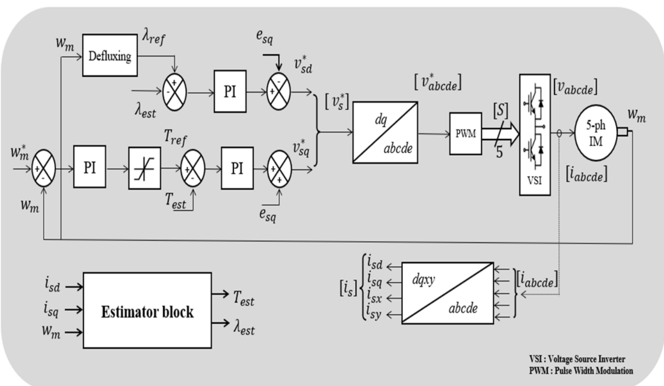

Fig. 4 Block diagram of IRFOC for the 5-phase IM

The validation of the vehicle drivetrain operation in healthy mode is carried out at a reduced power using a load torque of $10\ N\cdot m$ at time $t=0.07\ s$, and a velocity profile as shown in Fig. 5. Indeed, the velocity machine followed well the velocity profile before or after applying the load torque.

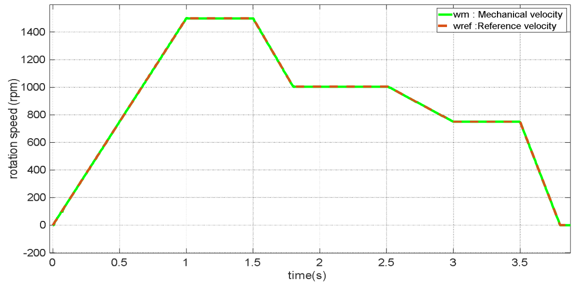

Fig. 5 Velocity response of 5-phase IM

In addition, Fig. 6 shows that the electromagnetic torque provided by the five-phase induction machine follows well the applied load torque in the steady state of the velocity mission profile.

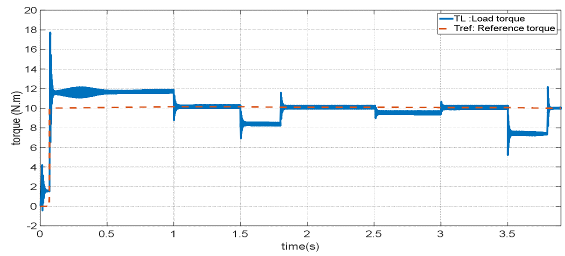

Fig. 6 Torque response of 5-phase IM

As shown in Fig. 7, we notice that the phase current's evolution is image of the velocity profile given in Fig. 5. Indeed, the phase currents are shifted by $\vartheta={}^{2\pi}/_{5}$, which corresponds to shift between each two stator phases.

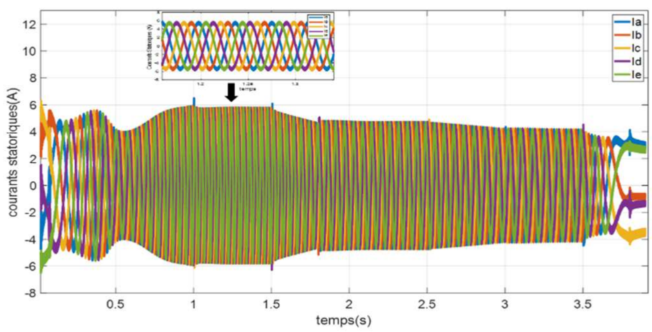

Fig. 7 Stator currents response of 5-phase IM

III. Multiphase System Analysis under VSI Open Phase Fault and Diagnostic Variables Selection's

A. *Open phase fault creation scenarios*

For a five-phase induction machine, the total number of faults, of an open arm type on the inverter side, that it can tolerate during operation is two faults. Thus, we can distinguish two scenarios of fault occurrence:

- The first scenario consists of creating one open-circuit per arm at each time. In this case, there are six classes, where one is dedicated to the healthy operation mode and the others for the remaining open-circuit arm related to the other phases of the five-phase induction machine.

- In the second scenario, two open-circuit faults are created simultaneously. In this case, there are 15 classes, where one class for healthy operation mode, five for a single open circuit fault at each time; and the others for two open-circuit faults at each time.

In this paper, we will focus only on the first scenario to create a single fault-circuit per arm at each time. In addition, a fault diagnosis will be carried out in order to develop a Faut Detection and Isolation algorithm using Neural Network approach.

B. *Selection of diagnostic variables*

To illustrate the effect of the OC fault on the dynamic behavior of the vehicle drivetrain, we have created the following OC faults based on first scenario: OC Arm_1: from $t = 1\ s$ to $t = 1.5\ s$, OC Arm_2: from $t = 1.5\ s$ to $t = 2\ s$, OC Arm_3: from $t = 2\ s$ to $t = 2.5\ s$, OC Arm_4: from $t = 2.5\ s$ to $t = 3\ s$; OC Arm_5: from $t = 3\ s$ to $t = 3.5\ s$.

We noticed the open circuit has affected the velocity response (Fig. 8) creating a short velocity drop with oscillations around the steady value. Similarly, the motor torque response (Fig. 9) shows the effect of the same open circuit where we notice high oscillations around the steady state value. For current responses (Fig. 10), we noticed that the waveforms are deformed differently depending on the location of the faults. Finally, the diagnosis we will focus only on the variables that describe the state of the arms of the inverter. Indeed, the fault impact in currents is more significant comparing to the other variables.

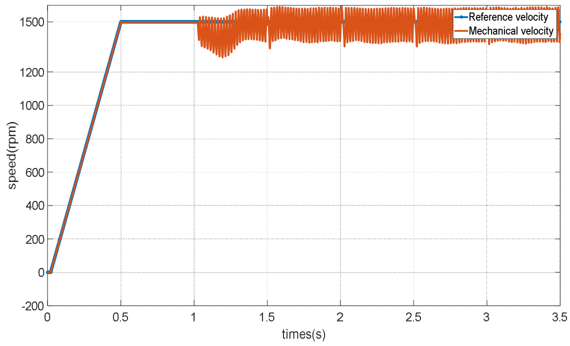

Fig. 8 Velocity response under OC faults

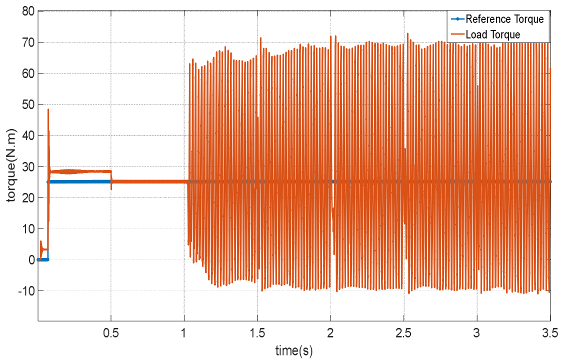

Fig. 9 Torque response under OC faults

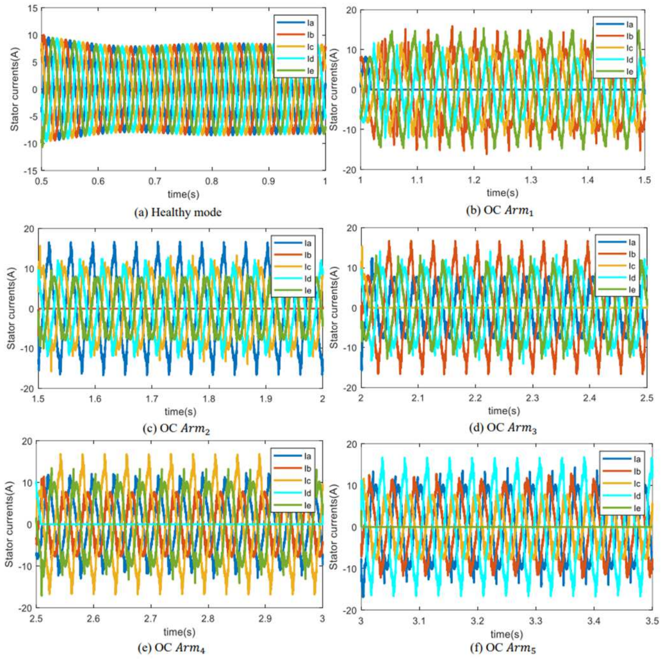

Fig. 10 Stator currents response under OC faults

The variables that are used for the diagnosis are the currents of the stator phases because they make it possible to detect and locate the open circuit faults of the inverter arms. In addition, as the current measurements are available for the control part, we can finally use them for diagnosis without adding other sensors.

C. *Establishment of the $I_\alpha - I_\beta$ characteristics*

The output current data measured from the induction machine I_a, I_b, I_c, I_d and I_e are transformed from the original 5-phase plane to a two-phase I_α and I_β plane using the Concordia transformation. This transformation is performed for the evaluation of the stator current patterns of the machine when OC faults occur.

The matrix which makes it possible to perform this transformation is given by:

$$C_{5/2} = \frac{2}{5}\begin{bmatrix} 1 & \cos(\vartheta) & \cos(2\vartheta) & \cos(3\vartheta) & \cos(4\vartheta) \\ 0 & \sin(\vartheta) & \sin(2\vartheta) & \sin(3\vartheta) & \sin(4\vartheta) \end{bmatrix} \quad (30)$$

With $\vartheta = {}^{2\pi}/_{5}$ is the angle between the phases of the machine. Under healthy operating mode, the characteristic of the currents $I_\alpha - I_\beta$, obtained from the Concordia transformation describes a circle, whereas, in the event of faults, this characteristic of the currents $I_\alpha - I_\beta$ is deformed in two directions, because each inverter arm is linked to a power stage which consists of two transistors. Fig. 11 gives the characteristic $I_\alpha - I_\beta$ in healthy mode and faulty mode for each scenario.

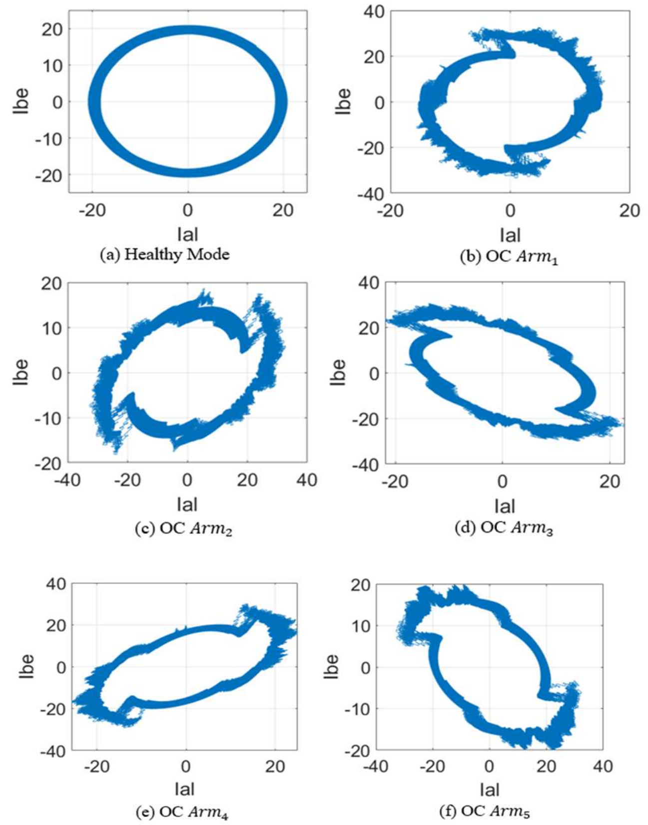

Fig. 11 Characteristic $I_\alpha - I_\beta$ for each operating mode

IV. Proposed Real-Time FDI Algorithm

A. Structure of the proposed Real-time FDI algorithm

The structure of the proposed algorithm for the detection and localization of faults is composed of the five-phase induction machine, the control part, the fault generation, the extraction system and the MLP neural network. The extraction system feeds the MLP network with significant characteristics that allow it to make the decision on the presence of an OC fault as well as its location. The extraction system part and the MLP network will be detailed in the following sections. Fig. 12 gives a simplified structure of the diagnosis system.

B. Feature extraction

For a better classification, an extractor of the characteristics remains mandatory. The accuracy and speed of the MLP neural network depends on the ability of the extractor system to provide meaningful detail across all possible classes.

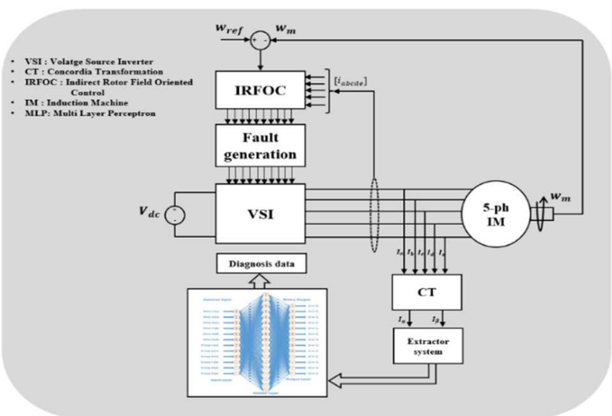

Fig. 12 Diagnosis system structure

The feature extraction system must meet the following properties:

- To provide the neural network with details to quickly detect the fault.
- To locate of each model class between the limits defined by a threshold.
- To make the characteristic extractor universal for different reference speeds by standardized functions.

According to the literature, many signal-processing methods have been applied for pre-processing for fault recognition, including time-domain analysis, frequency-domain analysis, time–frequency analysis [19]. In this paper, the Fourier transform (FT) is used to extract the main characteristics provided by the currents $I_\alpha - I_\beta$.
Figure 13 shows that the stator currents period remains the same before and after the occurring of the fault.

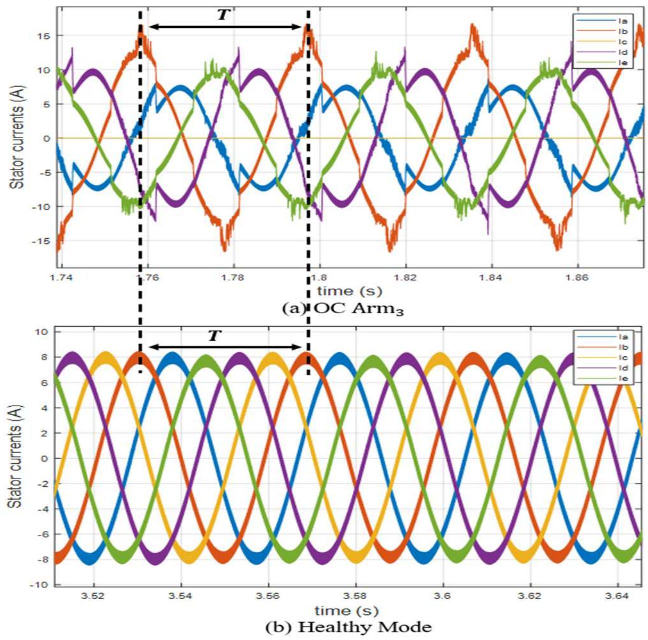

Fig. 13 Stator currents period

This period T is given by:

$$f_1 = \frac{1}{T} = \frac{n \cdot p}{60} \qquad (31)$$

Where n and p are velocity machine and number of pole pairs respectively.

Fourier transform applied to the currents $I_\alpha \; et \; I_\beta$ is given by:

$$I_\alpha(f) = TF\big(I_\alpha(t)\big) = \int_{-\infty}^{+\infty} I_\alpha(t) \cdot e^{-j2\pi f t} dt \qquad (32)$$

$$I_\beta(f) = TF\left(I_\beta(t)\right) = \int_{-\infty}^{+\infty} I_\beta(t) \cdot e^{-j2\pi f t} dt \qquad (33)$$

These transforms around the frequency f_1 are given by:

$$I_\alpha(f_1) = TF\big(I_\alpha(t)\big) = \int_{-\infty}^{+\infty} I_\alpha(t) \cdot e^{-j2\pi f_1 t} dt \qquad (34)$$

$$I_\beta(f_1) = TF\left(I_\beta(t)\right) = \int_{-\infty}^{+\infty} I_\beta(t) \cdot e^{-j2\pi f_1 t} dt \qquad (35)$$

By using the Euler's formula for real number x given by:

$$e^{jx} = \cos(x) + j \cdot sin(x). \qquad (36)$$

We obtain:

$$I_\alpha(f_1) = \int_{-\infty}^{+\infty} I_\alpha(t)\cdot\cos(2\pi f_1 t)\cdot dt - j\cdot\int_{-\infty}^{+\infty} I_\alpha(t)\cdot sin(2\pi f_1 t)\cdot dt \quad (37)$$

$$I_\beta(f_1) = \int_{-\infty}^{+\infty} I_\beta(t)\cdot\cos(2\pi f_1 t)\cdot dt - j\cdot\int_{-\infty}^{+\infty} I_\beta(t)\cdot sin(2\pi f_1 t)\cdot dt \quad (38)$$

For each quantity, we calculate the magnitudes A_α et A_β:

$$A_\alpha(f_1) = \sqrt{(\int_{-\infty}^{+\infty} I_\alpha(t)\cdot cos(2\pi f_1 t))^2 + (\int_{-\infty}^{+\infty} I_\alpha(t)\cdot sin(2\pi f_1 t))^2} \quad (39)$$

$$A_\beta(f_1) = \sqrt{(\int_{-\infty}^{+\infty} I_\beta(t)\cdot cos(2\pi f_1 t))^2 + (\int_{-\infty}^{+\infty} I_\beta(t)\cdot sin(2\pi f_1 t))^2} \quad (40)$$

These magnitudes are used to feed the perceptron multilayer neural network to detect and locate OC faults on the inverter side.

Figure 14 shows different classes that will be used to train the MLP system. Also, the same figure gives these magnitudes around the frequencies $3 * f_1$ and $5 * f_1$. We can notice that the information given by these two curves is less significant compared to that given by the Fourier transform at f_1.

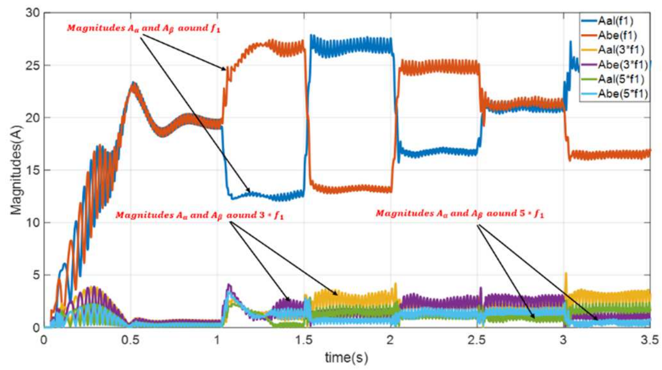

Fig. 14 Magnitudes A_α and A_β

C. *Multi-Layer Perceptron Neural Network Structure*

The Multilayer Perceptron MLP network is used for the detection and location of a single open circuit faults on VSI side.

In order to improve the algorithm accuracy and to avoid the overfitting, the MLP structure is optimized via an empirical approach, based on simulation, starting with a first structure of one hidden layer with 10 neurons, and ending with an optimal structure of 4 layers, as shown in figure 15. The 3 hidden layers are respectively consisted by 70, 90 and 80 neurons; while the output layer is consisted of two neurons, where the first neuron describes the operating mode (1: Healthy mode, and 0: Faulty mode), and the second one locates the fault, by giving the phase number from 1 to 5. The MLP input consists of two neurons which correspond to A_α and A_β.

The training process of the MLP network was carried out offline using Matlab code. First, for each created single fault on the VSI arms of the drivetrain simulator, a set of data was collected. Then, the optimization of the MLP network is performed, choosing the number of hidden layers and the number of neurons on each layer. Finally, the optimized MLP network is integrated online in the simulator, in order to test its robustness and its accuracy in the detection and localization of OC faults on the VSI arms.

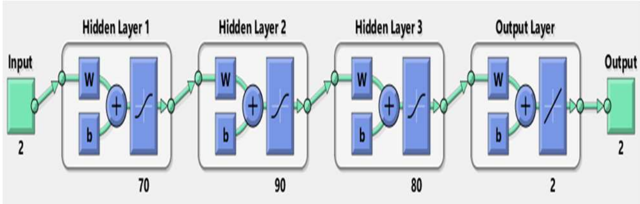

Fig. 15 MLP neural network structure

V. PERFORMANCES EVALUATION OF FDI ALGORITHM

The validation is carried out, using an arbitrary scenario, with the following OC faults occurrence on the inverter side: OC_ Arm 3 → OC_ Arm 5 → OC_ Arm 1; each fault is created in steady state for a duration of 0.4 s at 1500 rpm and a load torque of 25 Nm. Stator currents response to OC fault scenario are given in figure 16. In the first step, these currents are used to compute the magnitudes A_α and A_β using Fourier transform at the fundamental frequency f_1. Then the MLP neural network is fed using these magnitudes.

Figure 17 and figure 18 show the detection and location response of the MLP network. We can observe that the OC fault on the VSI side is promptly detected and located thanks to the robustness and accuracy of the proposed approach. Indeed, figure 19 shows the confusion matrix of the MLP network performance where the global accuracy reaches 97.4 %. The peaks that appear on the responses of the MLP network are due to the transition time from scenario to scenario, where the magnitudes A_α and A_β are not fixed (figure 14).

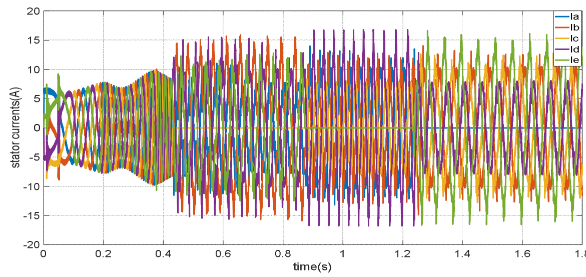

Fig. 16 Stator currents response under OC faults

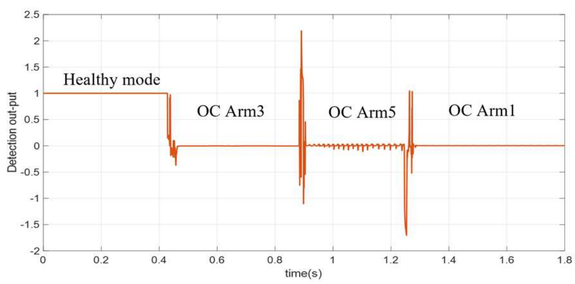

Fig. 17 Fault detection response of the neural network

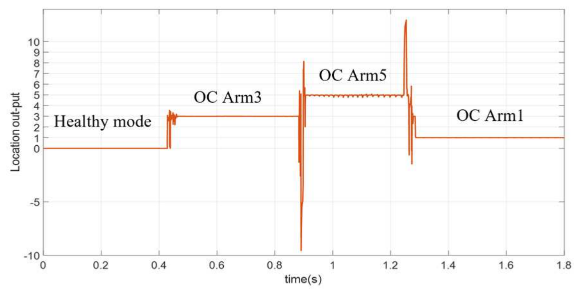

Fig. 18 Fault location response of the neural network

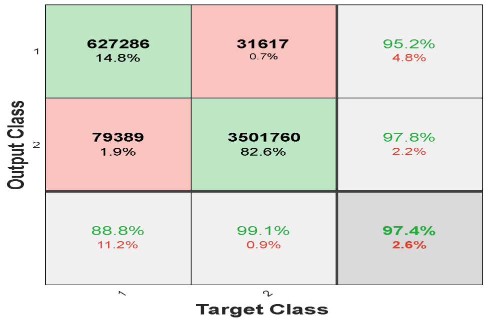

Fig. 19 Confusion matrix of the developed neural network

VI. Conclusion

In this paper, an automatic fault detection and location approach for any open phase fault in the VSI, feeding a 5-phase induction machine used in an electric vehicle drivetrain is developed and validated by simulation. This algorithm is developed using a MLP neural network and a feature extractor based on Fourier transform.

The advantages of this approach comparing to conventional FDI methods resides in its high fidelity to detect and to locate any OC fault in any arm of the VSI using only stator currents of the five phase induction machine. In addition, the accuracy to detect and to locate any OC fault is very high and the computing time of the algorithm is very fast to provide the results. Some perspectives to extend this approach consist to validate it for any operating point from the velocity operation range of the five phase induction machine and to validate it on a test bench to setup in our laboratory. Further work after the validation of the FDI consists to develop and to validate a fault tolerant control strategy in order to keep good performance in faulty operation mode and to ensure safety of the electric vehicle and the driver.

Appendix

TABLE I. Parameters of the five pase IM

Symbol	Quantity	Value
n	number of phases	5
R_s	stator resistance	12.85 Ω
R_r	rotor resistance	4.8 Ω
L_{lr}	rotor leakage inductance	79.93 mH
L_{ls}	stator leakage inductance	79.93 mH
M	mutual inductance	681.7 mH
p	Number of pole pairs	1
J_m	inertia	0.02 kg/m^2
B_m	viscous coefficient of friction	0.001 N.m.s./rad
V_{dc}	DC bus voltage	650 V
I_n	rated current	15 A
ω_{ref}	rated speed	1500 rpm
T_{max}	maximum torque	50 N.m

References

[1] M. J. Duran, E. Levi, and F. Barrero, "Multiphase electric drives: introduction," in Wiley Encyclopedia of Electrical and Electronics Engineering, 2017, pp. 1-26.

[2] E. Levi, "Multiphase electric machines for variable-speed applications," in IEEE Transactions on Industrial Electronics, vol. 55, no. 5, pp. 1893-1909, May 2008.

[3] Duc Tan VU, Fault-tolerant control of non-sinusoidal multiphase permanent magnet synchronous machine drives under constraints on current and voltage for automotive applications, Phd Thesis ENSAM ParisTech Campus of Lille, November 2020.

[4] R. Bojoi, S. Rubino, A. Tenconi, and S. Vaschetto, "Multiphase electrical machines and drives: A viable solution for energy generation and transportation electrification," in International Conference and Exposition on Electrical and Power Engineering (EPE), Iasi, Romania, 2016, pp. 632-639.

[5] Y. SAADI, Stratégies de contrôle et analyse des défauts d'une Machine à Réluctance Variable pour une chaîne de traction électrique, Thèse de doctorat de l'Université Paris-Saclay Préparée à l'Université Paris-Sud, Juillet 2019.

[6] David G Dorrell, Andrew M Knight, Mircea Popescu, Lyndon Evans, and David A Staton. Comparison of different motor design drives for hybrid electric vehicles. In Energy Conversion Congress and Exposition (ECCE), 2010 IEEE, pages 3352–3359. IEEE, 2010.

[7] N. K. Nguyen, E. Semail, F. Meinguet, P. Sandulescu, X. Kestelyn and B. Aslan, "Different virtual stator winding configurations of open-end winding five-phase PM machines for wide speed range without flux weakening operation," 2013 15th European Conference on Power Electronics and Applications (EPE), 2013, pp. 1-8, doi: 10.1109/EPE.2013.6634346

[8] R. Bojoi, S. Rubino, A. Tenconi, and S. Vaschetto, "Multiphase electrical machines and drives: A viable solution for energy generation and transportation electrification," in International Conference and Exposition on Electrical and Power Engineering (EPE), Iasi, Romania, 2016, pp. 632-639.

[9] E. Semail, A. Bouscayrol, and J. P. Hautier, "Vectorial formalism for analysis and design of polyphase synchronous machines," Eur. Phys. J. AP, 10.1051/epjap:2003034 vol. 22, no. 3, pp. 207-220, 2003.

[10] Z. Liu, Y. Li and Z. Zheng, "A review of drives techniques for multiphase machines," in CES Transactions on Electrical Machines and Systems, vol. 2, no. 2, pp. 243-251, June 2018, doi: 10.30941/CESTEMS.2018.00.

[11] A. Bhuiyan, Md. Maeenul, Sajal K. Das, F. Ali, Z. Tasneem, R. Islam, D. K. Saha, Md F. R. Badal, Md H. Ahmed, S. I. Moyeen, A Survey on Fault Diagnosis and Fault Tolerant Methodologies for Permanent Magnet Synchronous Machines, Article in International Journal of Automation and Computing · August 2020.

[12] S. Yakoub, R. Sehab, A. Chaibet, M. Boukhnifer, et D. Diallo, An Automatic Fault Detection and Localization Strategy for Switched Reluctance Machine Open Circuit Fault in EVs Applications. IEEE International Conference on Control, Automation and Diagnosis, ESTACA, pp. 1-6, 2019.

[13] Alyoussef, F.; Akrad, A.; Sehab, R.; Morel, C.; Kaya, I. Velocity sensor fault-tolerant controller for induction machine using intelligent voting algorithm. Energies 2022, 15, 3084.

[14] R. Liu, B. Yang, E. Zio, X. Chen, Artificial intelligence for fault diagnosis of rotating machinery: A review, Mechanical Systems and Signal Processing, Volume 108, 2018, Pages 33-47.

[15] Furqan Asghar, Muhammad Talha, Sung Ho Kim, "Neural network based fault detection and diagnosis system for three-phase inverter in variable speed drive with induction motor", Journal of Control Science and, Engineering vol. 2016, 12 pages, 2016.

[16] Mario BERMÚDEZ GUZMÁN, Novel control techniques in multiphase drives: direct control methods (DTC and MPC) under limit situations, Phd Thesis, ENSAM ParisTech Campus of Lille, December 2018.

[17] F. Barrero and M. J. Duran, "Recent advances in the design, modeling, and control of multiphase machines—Part I," in IEEE Transactions on Industrial Electronics, vol. 63, no. 1, pp. 449-458, Jan 2016.

[18] M. J. Duran and F. Barrero, "Recent advances in the design, modeling, and control of multiphase machines—Part II," in IEEE Transactions on Industrial Electronics, vol. 63, no. 1, pp. 459-468, Jan 2016.

[19] R. Liu, G. Meng, B. Yang, C. Sun, X. Chen, Dislocated time series convolutional neural architecture: an intelligent fault diagnosis approach for electric machine, IEEE Trans. Ind. Infor. 13 (3) (2017) 1310–1320